This is a repository copy of *A wireless fluorescent flexible force sensor based on aggregation-induced emission doped liquid crystal elastomers*.

White Rose Research Online URL for this paper:
https://eprints.whiterose.ac.uk/209698/

Version: Accepted Version

This is an author produced version of an article published in Soft Matter. Uploaded in accordance with the publisher's self-archiving policy.

10.1039/D3SM01715J

Soft Matter

A Wireless Fluorescent Flexible Force Sensor Based on Aggregation-Induced Emission Doped Liquid Crystal Elastomers

Xiaoxue Du, [a,c] Yanjun Liu, [a] Dongyu Zhao, [d,*] Helen F. Gleeson [c,*] and Dan Luo [a,b,*]

Flexible strain sensors have drawn a lot of interest in various applications including human mobility tracking, rehabilitation/personalized health monitoring, and human-machine interaction, but suffer from interference of electromagnetic (EM). To overcome the EM interference, flexible force sensors without sensitive electronic elements have been developed, with drawbacks of bulky modules that hinders their applications in remote measurement with power-free environment. Therefore, it is highly desirable to fabricate a compact wireless flexible force sensor but it is still a challenge. Here, we demonstrate a fluorescent flexible force sensor based on aggregation-induced emission (AIE) doped liquid crystal elastomer (LCE) experimentally. The proposed force sensor film can be used to measure force through the variation of fluorescent intensity induced by the extension or contraction of LCE film, which leads to reduce or increase of the aggregation degree of AIE molecules within. This compact wireless force sensor features lightweight, low-cost, high flexibility, passivity and anti-EM interference, which also enables the naked eye observation. The proposed sensor provides inspiration and a platform for a new concept of non-contact detection, showing application potential in human-friendly interactive electronics and remote-control integration platform.

INTRODUCTION

Flexible strain sensors have drawn a lot of interest in various applications including human mobility tracking [1,2], rehabilitation/personalized health monitoring [3,4], and human-machine interaction [5,6]. Several materials such as polyimide (PI) [7-9], polyurethane (PU) [10], polyethylene terephthalate (PET) [11,12], polydimethylsiloxane (PDMS) [13] and organic transistors [7, 14-15] have been used to fabricate flexible force sensors, where the high flexibility of materials enable the sensor to resist the damage from physical shape changing. Due to the existence of sensitive circuit with capacitive or inductive design, the usage of those flexible sensors would be influenced by the interference of electromagnetic (EM). To overcome the EM interference, flexible force sensor based on PET [16] and PDMS [17-19] without sensitive electronic elements have been developed, which mainly utilize resistive circuit, piezoelectric device or non-circuit design (for example optical signal acquisition). However, all abovementioned sensors require power supply either are

wire-connected, or with bulky modules (batteries or wireless communication) for remote operation, which hinders their applications in remote measurement with power-free environment. Therefore, it is highly desirable to fabricate a compact wireless flexible force sensor but it is still a challenge. As a smart responsive material, liquid crystal elastomer (LCE) has attracted significant attention in soft robots [20, 21], actuators [22-26], and fibers [27]. LCE is also very suitable for flexible force sensor due to its soft elasticity, reversible deformation, and anisotropic mechanical and optical response. The ionic liquid can be doped into LCE to form an ionic conductive elastomer with potential of force sensing, whereas it can only switch between transparent, blue, and opaque during the tension-release [28]. Recently, a photoelastic strain sensor based on acrylate-based isotropic LCE with high strain-optic coefficients and high compliances has been proposed and provides a potential solution for compact wireless flexible force sensor [29]. However, this method requires assistance of polarizers as well as complicated calculation of birefringence and order parameter, which is not simple and easy to use.

Aggregation-induced emission (AIE) [30] materials have been extensively explored in diverse fields including sensor, [31] and biomedical applications [32-34]. Due to its extraordinary property in photophysics, the AIE fluorogens are extremely emissive in aggregation because of the restriction of rotation within the molecule, which is the contrary of aggregation-induced quenching [35-37]. Several attempts based on combination of AIE-LCE material have been investigated in field such as fluorescence display [38-40], ions detection [41], temperature sensor [42-44] and actuation capability sensing

a. Department of Electrical and Electronic Engineering, Southern University of Science and Technology, Shenzhen, 518055, China.
b. Guangdong Provisional Key Laboratory of Functional Oxide Materials and Devices, Southern University of Science and Technology, Shenzhen 518055, China.
c. School of Physics and Astronomy, University of Leeds, Leeds, LS2 9JT, UK
d. School of Chemistry and Environment, Beihang University, Beijing, 100191, China.
* Corresponding authors.

[45]. It is expected that AIE luminogens can enable fluorescence in LCE force sensor by providing wireless capability in naked-eye observation.

In this paper, we investigate a fluorescent force sensor based on AIE doped LCE experimentally. The proposed force sensor film can be used to measure force through the variation of fluorescent intensity induced by the extension or contraction of LCE film, which leads to reduce or increase of the aggregation degree of AIE molecules within. This compact wireless force sensor features lightweight, low-cost, high flexibility, passivity and anti-EM interference, which also enables the naked eye observation. The proposed sensor provides inspiration and a platform for a new concept of non-contact detection, showing application potential in human-friendly interactive electronics and remote-control integration platform.

MATERIALS AND METHODS

The liquid crystal material 1,4-Bis-[4-(3-aryloyloxypropyloxy) benzoyloxy]-2-methylbenzene (RM257, 95%) was provided by Nanjing Leyao Technology Co. Ltd. (China). Pentaerythritol tetrakis (3-mercaptopropionate) (PETMP, $\geq$ 95%) was purchased from Shanghai D&B biological Science and Technology Co. Ltd. (China). 2,2'-[1,2-Ethylenedioxy] diethanethiol (EDDET, 95%) and Dipropylamine (DPA, 99%) were obtained from Macklin (China). N,N-Dimethylformamide (DMF) was purchased from Shanghai Lingfeng Chemical Reagent Co. Ltd. (China). The TPE-PPE, as the AIE material here, was supplied by Beihang University. The chemical structures of RM257, PETMP, EDDET, DPA and TPE-PPE are shown in Figure 1. The fluorescence intensity was obtained from processing the images, which were captured by a digital single lens reflex (SLR) camera (Nikon D7100), where the shutter speed of the digital SLR camera was 1/60 s and the ISO sensitivity was ISO 1250 (ISO is short for International Organization for Standardization). The fluorescence spectrum was obtained by microspectrophotometer (CRAIC technologies Inc.). The mixtures were treated by the mixer from SCILOGEX (MX-S). The Milli-Q water purification system (Millipore, Bedford, MA) was operated to prepare all aqueous solutions with DI water.

The preparation method of the LCE sample was based on two-step crosslinking with a small amplitude change [46-48]. In general, the stretchability of a LCE is closely related to its

crosslinking degree [49]. In order to obtain a greater tensile capacity, two-step crosslinking method was adopted in our later experiments but only the first step of crosslinking reaction was carried out. The composition of the fluorescent LCE was shown as Table 1. These materials were applied to making the sensor relative to the following process. Firstly, 1236.08 mg (2.10 mmol) RM257 and 0.60 mg TPE-PPE was dissolved into 1 ml DMF, and heated to 85 ˚C for the purpose of hydrotropism. After cooling to room temperature, 277.10 mg (1.52 mmol) of spacer EDDET and 117.28 mg (0.24 mmol) of cross-linker PETMP were added to form the RM mixture. On the other side, the catalyst DPA was dissolved into DMF to form a DPA-DMF solution with a 2% (v/v) concentration of DPA. After the RM mixture had been dissolved completely, 250 µl of the prepared 2% (v/v) catalyst DPA-DMF solution was added into the RMs mixture to catalyze the polymerization. The dilution of DPA is to prevent the catalytic reaction from being too violent and causing heterogeneous polymerization. Then, the mixture was treated by the mixer to ensure even mixing. After that, the mixture was cast into a rectangular Teflon mold (25 mm × 3 mm × 1 mm) and degassed for 5 min. Later, the mixture was solidified in the mold at room temperature for 24 hours. Finally, after drying in an oven at 85 ˚C for solvent evaporation and cooling down in the room temperature, a loosely cross-linked LCE was achieved.

Table 1 The composition of the fluorescent LCE.

	Main chain	Crosslinker	Extender	Catalyst	AIE
Chemicals	RM257	PETMP	EDT	DPA	TPE-PPE
Mole concentration	54.40 mol%	6.22 mol%	39.38 mol%	/	/
Weight or volume	1236.08 mg	277.10 mg	117.28 mg	5 µl	0.60 mg

RESULTS AND DISCUSSION

The mechanism of proposed force sensor is derived from the variation of the fluorescence intensity caused by the changes in the degree of aggregation due to stretching. Figure 2 demonstrates the schematic diagram of the fluorescent force sensor based on aggregation-induced emission (AIE) doped LCE film. The structure of sensor is shown in Figure 2a. At the original state, the AIE doped LCE film is bright due to aggregation of TPE-PPE. When an external force is applied, the fluorescent LCE film will be stretched or extended, leading to dim state due to a reduction in the aggregation degree of TPE-PPE (as shown in Figure 2b). Therefore, the fluorescence
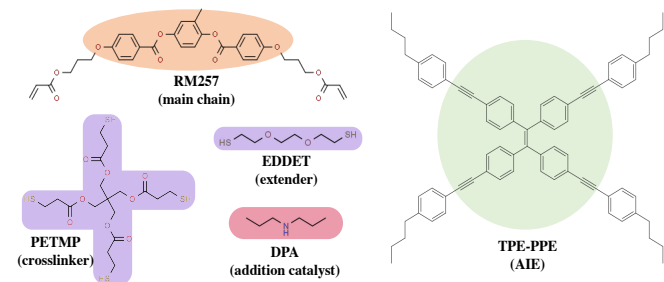
Figure 1 Chemical structures of RM257, PETMP, EDDET, DPA and TPE-PPE used in the formation of fluorescent liquid crystal elastomers.
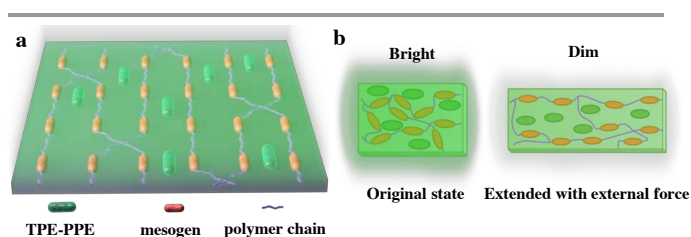
Figure 2 (a) The schematic diagram of the fluorescent force sensor based on AIE doped LCE film. (b) Fluorescence states before and after an external force.
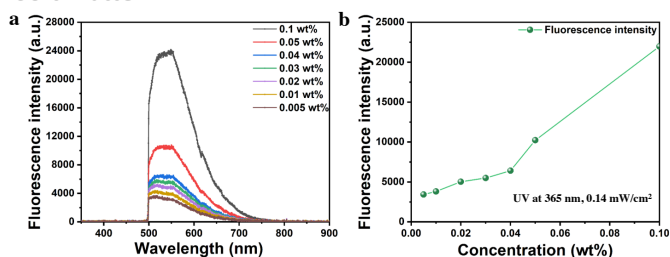
Figure 3 (a) Fluorescence spectrum for mixtures with different concentrations of TPE-PPE. (b) The fluorescence intensity at 520 nm versus concentration of TPE-PPE of mixtures.
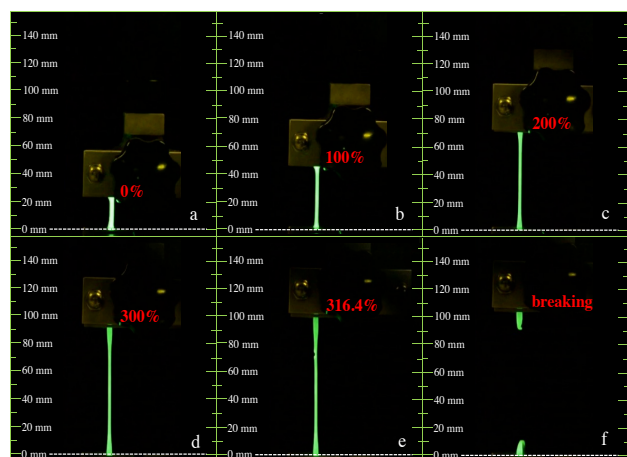
Figure 4 The tensile stress-strain performance of fluorescent LCE film in a tensile-testing machine while excited by a UV light (365 nm, 0.84 mW/cm^2) at different strain states.

intensity of the sensor is related to the external force and thus can be used to measure the applied force, which enables a sensitive non-contact force measurement and provides a lot of potential applications in biosensors and interactive electronics. To investigate the property of AIE-activation and the relationship between the concentration and photoluminescence (PL), several mixture samples with different concentrations of AIE luminogen TPE-PPE were prepared and tested. Considering both the fluorescence changing and the TPE-PPE's usage, the concentration of TPE is selected to be as small as possible while ensuring the change in fluorescence intensity is sufficiently obvious during stretching. Figure 3a demonstrates the fluorescence spectrum for seven mixtures with different TPE-PPE concentration from 0.005wt% to 0.01 wt%, respectively. It can be seen that with increasing of TPE-PPE concentration, the highest fluorescence intensity of the mixtures under ultraviolet (UV) excitation increases from 3432 (a.u.) to 21971 (a.u.) (as shown in Figure 3b). From the theoretical point of view, the essence of AIE is the inhibition of non-radiation attenuation and enhance of fluorescence production. The stretching of LCE film will decrease the aggregation of fluorogens in the networks, leading to an enhance of non-radiation attenuation and a decrease of aggregation emission. As the LCE film will be stretched up to approximately 4 times of its original length as force sensor, the variation of fluorescence intensity should be obvious under the stretching. Therefore, the mixture with middle TPE-PPE concentration of 0.05 wt% was chosen in the following experiments.

Because only the first step crosslinking reaction was carried out from the two-step crosslinking method, the obtained LCE film possesses a greater tensile capacity than normal LCE made by the completed two-step crosslinking method. Figure 4a-4e shows the photographs of fluorescent LCE film for tensile stress-strain performance testing in a tensile-testing machine (Qunlong QLW-5E) while excited by a UV light (365 nm, 0.84 mW/cm^2) at different strain states from original 0% to 316.4%, respectively, where the length of original fluorescent LCE was L_0=23.36 mm, with width of 3.01 mm and thickness of 1.33 mm. Beyond strain of 316.4%, the LCE will be broken to two parts, as shown in Figure 4f.

According to the definition of the tensile strain [50], S_{strain} can be expressed as:

$$S_{strain} = \frac{(L-L_0)}{L_0} \times 100\% , \qquad (1)$$

where L is the final length of the LCE and the L_0 is the original length of the LCE. The tensile stress S_{stress} can be described as [50]:

$$S_{stress} = \frac{F}{Wt} , \qquad (2)$$

where F is the force applied to the LCE, W is the width of the LCE, and t is the thickness of the LCE sample at the cutter area. The relationship of stress/force (red/blue curve) versus strain of the LCE force sensor is plotted in Figure 5a. It can be seen that, when the strain increases from 0% to maximum of 316.4%, the force increases from 0 N to 9.64 N (0 g to 983.67 g, 1 g = 9.8 N/kg), and the corresponding stress increases from 0 MPa to 2.246 MPa. Here, the date of force is measured by the tensile-testing machine (Qunlong QLW-5E), and the data of strain and stress are calculated according to Eq. 1 and 2 based on measured length. When exposed to UV illumination (365 nm, 0.84 mW/cm^2), the LCE will present green fluorescence. The changing process of the LCE's fluorescence intensity can be recorded into a video by a digital single lens reflex camera, and the fluorescence intensity at each stage can be extracted through a code program. This method is letting the loop code catch fluorescence intensity from the video each 0.1 s. After reading the fluorescence intensity at each stage, the "strain-force" curve (orange) is used to compare with the "strain-fluorescence" curve (cyan), as shown in Figure 5b. It can be seen that, with the increase of fluorescence intensity, the corresponding force of sensor decreases. The relationship between the force and fluorescence can be extracted from the point-point data, which can be applied in predicting the value of force from the obtained intensity fluorescence in similar experimental environments, as plotted in Figure 5c. The logistic fitting curve of fluorescence intensity with goodness of R^2=0.99 is obtained based on the data in Figure 5c, leading to a predicted variation of the fluorescence intensity I:

$$I = 245.193 - 26.37 \times \left(1 - e^{-\frac{F}{25.60}}\right) - 61.22 \times \left(1 - e^{-\frac{F}{0.38}}\right) , \quad (4)$$

where F is the force applied to the LCE film, and I is the fluorescence intensity that the LCE presented under the UV exposure (365 nm, 0.84 mW/cm^2).

To test the accuracy of proposed fluorescent sensor, three objects including a billiard ball, a toy, and an orange in different weight. Based on the measured fluorescent intensity (Figure 6a-6c) of the LCE force sensor, the corresponding ΔI of the billiard ball, toy, and orange are 18.686, 30.047, and 37.645, respectively, corresponding to the calculated force of 0.3 N,
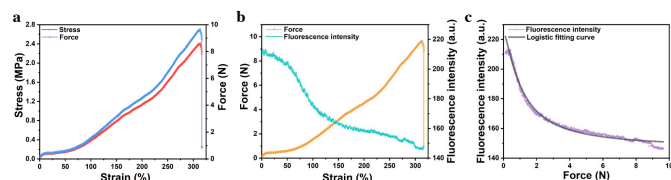
Figure 5 (a) The relationship of stress/force (red/blue curve) versus strain. (b) The relationship of force/fluorescence intensity (orange/cyan curve) versus strain. (c) The measured and fitting data of fluorescence intensity versus force.
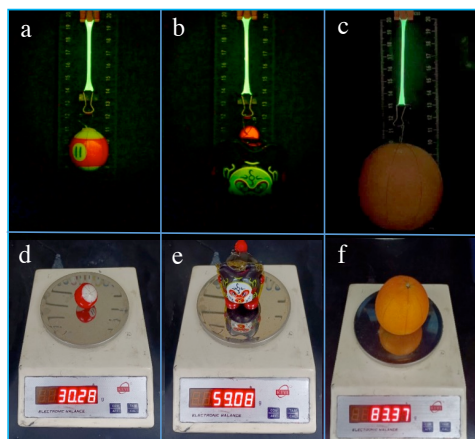
Figure 6 Photographs of fluorescent LCE force sensor for weighting (a) a billiard, (b) a toy, and (c) an orange. The corresponding measured weight based on fluorescence is 30.61 g, 60.20 g, and 83.97 g, respectively. The weight measured by a balance is (d) 30.28 g for the billiard, (e) 59.08 g for the toy, and (f) 83.37 g for the orange, respectively.

0.59 N, and 0.823 N according to Eq. 4. Therefore, the calculated weight of the billiard ball, toy, and orange are 30.61 g, 60.20 g, and 83.97g, respectively. Figure 6d-6f demonstrated the photography of the billiard ball, toy, and orange on the balance for weight measurement, showing the weights of 30.28 g, 59.08 g, and 83.87 g, respectively, with errors of 0.33 g (1.09%), 1.12 g (1.86%), and 0.10 g (0.12%). It worth mention that, larger force (or weight) measurement can be realized by directly increase the weight of LCE film or simply combine several films together.

Conclusions

In summary, a fluorescent force sensor based on AIE doped LCE has been explored experimentally. The relationship of fluorescence and loading force has been investigated. The proposed force sensor film can be used to measure force in range of 0 N to 9.64 N (0 g to 983.67 g), with features of lightweight, low-cost, high flexibility, passivity and anti-EM interference. The proposed sensor provides inspiration and a platform for a new concept of non-contact detection, showing application potential in human-friendly interactive electronics and remote-control integration platform.

Conflicts of interest

There are no conflicts to declare.

Acknowledgements

Notes and references

1   J. J. Park, W. J. Hyun, S. C. Mun, Y. T. Park, O. O. Park, *ACS Appl. Mater. Inter.,* 2015, **7**, 6317-6324.
2   Y. Khan, A. E. Ostfeld, C. M. Lochner, A. Pierre, A. C. Arias, *Adv. Mater.,* 2016, **28**, 4373-4395.
3   M. A. Darabi, A. Khosrozadeh, Q. Wang, M. Xing, *ACS Appl. Mater. Inter.,* 2015, **7**, 26195-26205.
4   Y. Cheng, R. Wang, J. Sun, L. Gao, *Adv. Mater.,* 2015, **27**, 7365-7371.
5   C. Wang, X. Li, E. Gao, M. Jian, K. Xia, Q. Wang, Z. Xu, T. Ren, Y. Zhang, *Adv. Mater.,* 2016, **28**, 6640-6648.
6   S. Yang, Y. C. Chen, L. Nicolini, P. Pasupathy, J. Sacks, B. Su, R. Yang, D. Sanchez, Y. Chang, P. Wang, D. Schnyer, D. Neikirk, N. Lu, *Adv. Mater.,* 2015, **27**, 6423-6430.
7   T. Someya, Y. Kato, T. Sekitani, S. Iba, Y. Noguchi, Y. Murase, H. Kawaguchi, T. Sakurai, *Proc. Natl. Acad. Sci. U.S.A,* 2005, **102**, 12321-12325.
8   K. Takei, T. Takahashi, J. C. Ho, H. Ko, A. G. Gillies, P. W. Leu, R. S. Fearing, A. Javey, *Nature Mater.,* 2010, **9**, 821–826.
9   D. Son, J. Lee, S. Qiao, R. Ghaffari, J. Kim, J. E. Lee, C. Song, S. J. Kim, D. J. Lee, S. W. Jun, S. Yang, M. Park, J. Shin, K. Do, M. Lee, K. Kang, C. S. Hwang, N. Lu, T. Hyeon, D-H. Kim, *Nature Nanotech.,* 2014, **9**, 397–404.
10 W. Hu, X. Niu, R. Zhao, Q. Pei, *Appl. Phys. Lett.,* 2013, **102**, 083303.
11 S. C. B. Mannsfeld, B. C-K. Tee, R. M. Stoltenberg, C. V. H-H. Chen, S. Barman, B. V. O. Muir, A. N. Sokolov, C. Reese, Z. Bao, *Nature Mater.,* 2010, **9**, 859–864.
12 G. Schwartz, B. C.-K. Tee, J. Mei, A. L. Appleton, D. H. Kim, H. Wang, Z. Bao, *Nat. Commun.,* 2013, **4**, 1859.
13 C. Pang, J. H. Koo, A. Nguyen, J. M. Caves, M-G. Kim, A. Chortos, K. Kim, P. J. Wang, J. B.-H. Tok, Z. Bao, *Adv. Mater.,* 2015, **27**, 634-640.
14 T. Someya, T. Sekitani, S. Iba, Y. Kato, H. Kawaguchi, T. Sakurai, *Proc. Natl. Acad. Sci. U.S.A,* 2004, **101**, 9966-9970.
15 S. C. B. Mannsfeld, B. C-K. Tee, R. M. Stoltenberg, C. V. H-H. Chen, S. Barman, B. V. O. Muir, A. N. Sokolov, C. Reese, Z. Bao, *Nature Mater.,* 2010, **9**, 859–864.
16 H. Tian, H. Shu, Y.-L. Cui, W.-T. Mi, Y. Yang, D. Xie, T.-L. Ren, *Nanoscale,* 2014, **6**, 699-705.
17 D. J. Lipomi, M. Vosgueritchian, B. C-K. Tee, S. L. Hellstrom, J. A. Lee, C. H. Fox, Z. Bao, *Nature Nanotech.,* 2011, **6**, 788–792.
18 C. Pang, G-Y. Lee, T. Kim, S. M. Kim, H. N. Kim, S-H. Ahn, K-Y. Suh, *Nature Mater.,* 2012, **11**, 795–801.
19 S. Jung, J. H. Kim, J. Kim, S. Choi, J. Lee, I. Park, T. Hyeon, D-H. Kim, *Adv. Mater.,* 2014, **26**, 4825-4830.
20 Y. Zhao, Q. Li, Z. Liu, Y. Alsaid, P. Shi, M. Khalid Jawed, X. He, *Sci. Robot.,* 2023, **8**, eadf4753.
21 T. J. White, Broer, D. J. *Nat. Mater.,* 2015, **14**, 1087–1098.

22 K. Dradrach, M. Zmyślony, Z. Deng, A. Priimagi, J. Biggins, P. Wasylczyk, *Nat. Commun.,* **2023**, 14, 1877.

23 S. Li, M. M. Lerch, J. T. Waters, B. Deng, R. S. Martens, Y. Yao, D.Y. Kim, K. Bertoldi, A. Grinthal, A. C. Balazs, J. Aizenberg, *Nature*, 2022, **605**, 76-83.

24 Y. Li, Y. Liu, D. Luo, *Adv. Opt. Mater.,* 2020, **9**, 2001861.

25 Y. Geng, R. Kizhakidathazhath, J. P. Lagerwall, *Nat. Mater.,* 2022, **21**, 1441-1447.

26 Z. Z. Nie, M. Wang, S. Huang, Z. Y. Liu, H. Yang, *Angew. Chem. Int. Ed.*, 2023, **62**, e202304081.

27 Q. Wang, X. Tian, D. Zhang, Y. Zhou, W. Yan, D. Li, *Nat. Commun.,* 2023, **14**, 3869.

28 Z. Y. Liu, Q. Jiang, H. K. Bisoyi, G. Q. Zhu, Z. Z. Nie, K. Jiang, H. Yang, Q. Li, *ACS Appl. Mater. Interfaces*, 2023, **15**, 28546-28554.

29 D. Mistry, M. Nikkhou, T. Raistrick, M. Hussain, E. Jull, D. L. Baker, H. F. Gleeson, *Macromolecules*, 2020, **53**, 3709-3718.

30 T. Y. Han, X. Feng, B. Tong, J. B. Shi, L. Chen, J. G. Zhi, Y. P. Dong, *Chem. Commun.,* 2012, **48**, 416–418.

31 C. W. T. Leung, Y. Hong, S. Chen, E. Zhao, J. W. Y. Lam, B. Z. Tang, *J. Am. Chem. Soc.,* 2013, **135**, 62-65.

32 Y. Yuan, C. Zhang, B. A. Liu, *Angew. Chem. Int. Ed.,* 2015, **54**, 11419–11423.

33 F. Hu, S. D. Xu, B. Liu, *Adv. Mater.,* 2018, **30**, 1801350.

34 Z. Y. Liu, H. Zou, Z. Zhao, P. F. Zhang, G. G. Shan, R. T. K. Kwok, J. W. Y. Lam, L. Zheng, B. Z. Tang, *ACS Nano.,* 2019, **13**, 11283–11293.

35 J. Luo, Z. Xie, J. W. Y. Lam, L. Cheng, H. Chen, C. Qiu, H. S. Kwok, X. Zhan, Y. Liu, D. Zhu, B. Z. Tang, *Chem. Commun.,* 2001, **18**, 1740-1741.

36 J. Chen, C. C. W. Law, J. W. Y. Lam, Y. Dong, S. M. F. Lo, I. D. Williams, D. Zhu, B. Z. Tang, *Chem. Mater.,* 2003, **15**, 1535-1546.

37 J. Mei, Y. Hong, J. W. Y. Lam, A. Qin, Y. Tang, B. Z. Tang, *Adv. Mater.,* 2014, **26**, 5429-5479.

38 D. Y. Zhao, F. Fan, J. Cheng, Y. L. Zhang, K. S. Wong, V. G. Chigrinov, H. S. Kwok, L. Guo, B. Z. Tang, *Adv. Opt. Mater.,* 2014, **3**, 199-202.

39 D. Y. Zhao, H. X. He, X. G. Gu, L. G, K. S. Wong, J. W. Y. Lam, B. Z. Tang, *Adv. Opt. Mater.,* 2016, **4**, 534-539.

40 D. Y. Zhao, W. H. Bi, B. Z. Tang, *Adv. Opt. Mater.,* 2021, **9**, 2100489.

41 X. X. Du, Y. J. Liu, F. Wang, D. Y. Zhao, H. F. Gleeson, D. Luo, ACS *Appl. Mater. Inter.,* 2021, **13**, 22361-22367.

42 W. L. Li, D. Huang, J. Wang, W. J. Shen, L. Z. Chen, S. Y. Yang, M. F. Zhu, B. Z. Tang, G. D. Liang, Z. X. Xu, *Polym. Chem.,* 2015, **6**, 8194-8202.

43 L. Liu, M. Wang, L. X. Guo, Y. Sun, X. Q. Zhang, B. P. Lin, H. Yang, *Macromolecules,* 2018, **12**, 4516–4524.

44 J. Wang, T. Wang, Q. Jiang, Y. P. Zhang, Y. Qiu, H. Wang, G. C. Yin, Y. G. Liao, X. L. Xie, *Macromol. Rapid Commun.,* 2022, **43**, e2200154.

45 Z. C. Jiang, Y. Y. Xiao, J. B. Hou, X. S. Chen, N. Yang, H. Zeng, Y. Zhao, *Angew. Chem. Int. Ed.,* 2022, **61**, e202211959.

46 H. Finkelmann, H. J. Kock, G. Rehage, *Makromol. Chem.,* 1981, **2**, 317-322.

47 T. H. Ware, M. E. McConney, J. J. Wie, V. P. Tondiglia, T. J. White, *Science,* 2015, **347**, 982-984.

48 Y. Xia, X. Zhang, S. Yang, *Angew. Chem. Int. Ed. Engl.,* 2018, **57**, 5665-5668.

49 T. J. White, D. J. Broer, *Nat. Mater.,* 2015, **14**, 1087-1098.

50 J. M. Gere, B. J. Goodno, Mechanics of materials. Cengage learning, Stamford, 2012, **1**, 30-31.